Received: 18 July 2017 | Revised: 12 February 2018 | Accepted: 8 April 2018 | Published on: 10 October 2018

DOI: 10.1002/qj.3311

RESEARCH ARTICLE

Quarterly Journal of the Royal Meteorological Society RMetS

Mesoscale rainfall patterns observed around wetlands in sub-Saharan Africa

Christopher M. Taylor[1,2] | Catherine Prigent[3] | Simon J. Dadson[4]

[1]Centre for Ecology and Hydrology, Wallingford, UK
[2]National Centre for Earth Observation, Wallingford, UK
[3]LERMA, Observatoire de Paris, PSL Research University, CNRS, Sorbonne Universités, Paris, France
[4]School of Geography and the Environment, University of Oxford, Oxford, UK

Correspondence
Christopher M. Taylor, Centre for Ecology and Hydrology, Benson Lane, Crowmarsh Gifford, Wallingford, Oxfordshire, OX10 8BB, UK.
Email: cmt@ceh.ac.uk

Funding information
Natural Environment Research Council, NE/I01277X/1.

Wetlands are dynamic components of the landscape, responding to local and upstream rainfall, river flow and groundwater variability, and to water management. At the same time, in regions of strong evaporative demand, wetlands can present very strong land surface heterogeneity to the atmosphere, driving marked gradients in sensible and latent heat fluxes. At certain times of year, wetlands can therefore potentially provide a land surface feedback on rainfall. Here we assess the influence of wetlands on rainfall across sub-Saharan Africa (SSA). Using a well-established multi-satellite based product of wetland extent with monthly temporal resolution, we find significant wetland coverage (>10%) occurs at some point in the 15-year dataset for about 22% of SSA. We analyse rainfall patterns in the vicinity of major wetlands using satellite data, and find a consistent signal across SSA of locally suppressed rainfall over the wetlands as compared to nearby drier areas. This signal contrasts with a simple atmospheric water balance perspective which would suggest increased rain in response to increased local evaporation. The observed signal is strongest during the afternoon and weakens overnight. Using cloud-top temperature data from the Sahel, we find that afternoon convective initiation is favoured close to wetlands, consistent with forcing by a thermally induced circulation from gradients in sensible heat fluxes. We also find that in this region, where the vast majority of rainfall is associated with remotely triggered Mesoscale Convective Systems (MCS), convection weakens when these systems pass over wetlands. From this study, we conclude that wetlands across the range of climate zones spanning SSA influence rainfall patterns locally, and where MCS are an important component of rainfall, this influence can extend over a larger region, associated with the tracks of long-lived MCS.

KEYWORDS
African rainfall, convection, land–atmosphere interactions, wetlands

1 | INTRODUCTION

Wetlands constitute a key component of the tropical African landscape, providing important fluxes of water and carbon between the land and the atmosphere. It is estimated that wetland CH_4 emissions represent 20–40% of the global CH_4 budget, making them the largest single natural source of atmospheric CH_4 (Denman *et al.*, 2007). Wetlands also provide important benefits for aquatic and terrestrial ecosystems via water quality and elements of natural flood control (Acreman and Holden, 2013; Dadson *et al.*, 2017). In some wetland areas (e.g. the Sudd, the Niger Inland Delta) evaporative losses from large inundated regions now and in the future may constrain water availability in rivers downstream (Mohamed *et al.*, 2006). In areas with strong seasonal and interannual hydroclimatic variability, wetland inundation can exert a strong control on fluxes of heat and water at the land-surface. These fluxes can then feed back on rainfall at local and

regional scales (Taylor, 2010). When rivers flood the surrounding low-lying areas, as happens along many of Africa's rivers in response to large seasonal fluctuations in upstream rainfall and runoff, they can strongly perturb the fluxes of energy and water into the atmosphere. Total evapotranspiration from a wetland can in some cases approach and even exceed equivalent open water evaporation rates, depending on the effects of vegetation (Mitsch and Gosselink, 2015). These evaporative fluxes are accompanied by very small or even negative daytime sensible-heat fluxes. In the absence of flooding, on the other hand, sensible heat can play an important part in the daytime energy balance, at the expense of latent heating. The actual partition between these two fluxes depends strongly on vegetation cover and soil moisture, with high Bowen ratios over drier, sparsely vegetated semi-arid regions compared to tropical forest areas. These fluxes influence the properties of the planetary boundary layer (PBL); once flooded, the overlying PBL is likely to be cooler, shallower and moister than in its unflooded state due to the reduced Bowen ratio. How the resulting vertical profiles of temperature and humidity influence the development of convective rainfall has been the subject of many studies (e.g. De Ridder, 1997; Findell and Eltahir, 2003).

Alongside this one-dimensional (1D) perspective, one must account for the fact that wetlands tend to be spatially well-organised, due to the underlying topography and river flows. Large wetlands often exist within regions where the water balance is dominated by rainfall, drainage and evapotranspiration. This is in contrast to the wetland water balance, where lateral flows through the river network and groundwater are crucial. If the landscape generates wetland features on length-scales of 10 km upwards, mesoscale gradients in sensible heat flux can drive breezes in the daytime PBL (Segal and Arritt, 1992). Though relatively weak, the convergence induced by these circulations can provide favourable conditions for the initiation of deep convection (Pielke, 2001). Indeed, observations of deep clouds and rain have shown in a number of regions of the world that surface-induced circulations appear to be the dominant mechanism affecting the triggering of deep convection at the mesoscale (Negri *et al.*, 2004; Taylor *et al.*, 2011; Taylor, 2015).

Much of the above research has focused on the impacts of soil moisture, deforestation and irrigation. A smaller number of studies have looked at the impacts of natural wetlands on rainfall. One wetland that has been the subject of a number of regional atmospheric modelling studies, motivated by plans to divert the White Nile, is the Sudd in Southern Sudan. Assessing the climatic impact of draining the swamp, Mohamed *et al.* (2005) found that the wetland had a negligible effect on the water budget at the regional scale. They argued that during the wet season, the surrounding land is not particularly water-stressed, and so the addition of a relatively freely evaporating swamp has only a modest effect on heat and moisture fluxes into the atmosphere. In a subsequent modelling study, Mohamed *et al.* (2006) noted a slight increase in precipitation after draining the wetland, suggesting that there was "enhanced convection over the dried soils". Zaroug *et al.* (2013) similarly found almost no effect on rainfall at the large scale due to removing the wetland, but did simulate a 15% decrease in rainfall locally when replacing the wetland with bare soil.

A more detailed numerical modelling study of the atmospheric processes in response to a wetland was presented by Lauwaet *et al.* (2012). They focused on Lake Chad, a mixture of open water and swamps, which has varied considerably in extent over recent decades in response to climate and upstream water use (Coe and Foley, 2001). Comparing simulations with different lake extents, Lauwaet *et al.* (2012) calculated a doubling of rain over the lake and downwind (towards the northeast at low levels). Consistent with studies from the Sudd, they found little impact on rainfall elsewhere, and only slightly increased rain when averaged over a large region. They further investigated the impact of the lake on precipitation from remotely triggered Mesoscale Convective Systems (MCS), which contribute the vast majority of rainfall in the Sahel (Mathon *et al.*, 2002). The westward propagation of MCS relies on the contrasting temperature of the convectively generated cold pool ahead of the system compared to the ambient air (Houze, 2004). Above the lake, the air is cooler due to reduced sensible heat flux. As a result, the thermal contrast between the MCS cold pool and the ambient air is reduced above the lake, and the density current weakens. Lauwaet *et al.* (2012) argue that this mechanism results in a tendency for MCS to become "blocked" by the lake, resulting in reduced rainfall on the western side of the lake. They also highlighted a second mechanism affecting MCS rainfall due to enhanced lake-driven humidity advected downwind towards approaching systems. This plume of moister air provides additional convective available potential energy (CAPE), resulting in more intense updraughts to the east.

To our knowledge there have been two previous observational studies looking at the impact of natural wetlands on deep convection. Prigent *et al.* (2011) analysed the diurnal and seasonal variability of convection and wetland extent at large scale (5°) across the Tropics. Looking at regions where inundation is driven by non-local rainfall, they found evidence of enhanced convection during periods with reduced wetland area. In regions where wetlands are driven by "local" rainfall, they were unable to isolate feedback effects at this scale. In a spatially more detailed study, Taylor (2010) examined space–time variability in cloud-top temperatures around the Mali wetlands associated with initiating and propagating MCS. The extent of the Mali wetlands is primarily driven by non-local rainfall that fell several months previously, allowing a cleaner separation between cause and effect. The study showed enhanced convective initiation around the edge of the wetlands and suppression of convection over the wetland itself. Such a pattern is consistent with a "wetland breeze", favouring convective initiation in the associated convergence zones. A cold-cloud signal from additional MCS initiated

in the vicinity of the wetland during periods of peak inundation was clearly evident 200 km and several hours away, suggesting an impact of the wetland on remote as well as local rainfall.

The observational results contrast with some of the modelling studies mentioned above, which largely emphasise enhanced rain over the wetland. Based on the modelling studies, Lauwaet *et al.* (2012) suggest that "creating a large water body in a semi-arid environment is unlikely to produce a widespread precipitation increase". This may be true when considering rainfall at very large scales, but as shown with observations by Alter *et al.* (2015), the creation of freely evaporating areas (in this case, extensive irrigation in Sudan) can lead to substantial spatial redistribution of rainfall. Moreover, important questions have been raised about the use of coarse-resolution models (where convection is parametrized) to assess land–precipitation feedbacks (Hohenegger *et al.*, 2009; Taylor *et al.*, 2012; 2013). There is a tendency for many convection schemes to be overly sensitive to low-level moisture (favouring rain over a more freely evaporating surface), and to trigger rainfall too early in the day. Such unrealistic early triggering affects the development of the PBL and mesoscale circulations, and suppresses any preferential development of deep convection over drier surfaces. In this context, observations of convection and rainfall are key to evaluating the behaviour of coarse-resolution atmospheric models, and determining the sign and strength of feedbacks at different length-scales and environments.

In terms of the land surface, the net impact of a wetland on rainfall is likely to be a function of its spatial scale, and the contrast in sensible and latent heat fluxes with the surrounding area. The regional rainfall climatology will also affect how the wetland affects precipitation. For example, where rainfall totals are dominated by short-lived convective events, the impact of the wetland on triggering storms is expected to be key. On the other hand, where MCS deliver the majority of rain, the critical feedback processes may be quite distinct (Gantner and Kalthoff, 2010).

It is difficult to quantify the impact of wetlands on rainfall from observations alone. However, observations can be important in identifying the dominant feedback sign, and in what regions and seasons impacts appear to be important. This article seeks to address this issue, using satellite measurements in the vicinity of wetlands across sub-Saharan Africa (SSA). In particular, we document the spatial pattern of rain around wetlands at different phases of the diurnal and seasonal cycle. We examine whether there are any consistent rainfall structures associated with wetlands across Africa's varied climatic zones. We also explore the impact on these rainfall patterns of interannual variability in wetland extent. Finally, we use higher spatial and temporal resolution cloud-top temperature data to determine the impact of wetlands on different phases of the convective life cycle.

The satellite datasets are introduced in the next section, followed by a characterization of the spatial and temporal variability in sub-Saharan wetlands. Rainfall patterns around selected wetlands are examined on diurnal, seasonal and interannual time-scales in section 4. This is followed by a more detailed analysis of the life cycle of convection in the vicinity of wetlands in the Sahel. We finish with discussions about feedback processes and their representation in numerical models, followed by more general conclusions.

2 | DATA

2.1 | Wetland data

For this study we use a dataset based on a multi-sensor technique which provides estimates of surface water extent and dynamics at the global scale (Prigent *et al.*, 2007; 2012). The Global Inundation Extent from Multi-Satellites (GIEMS) benefits from the complementary sensitivities of different satellite instruments to surface characteristics (e.g. water, vegetation and soil), to minimize limitations and uncertainties related to measurements by each individual instrument. Passive microwave observations are particularly sensitive to the presence of surface water, even under vegetation canopies, and the inundation detection primarily relies on the passive microwave signal. However, additional observations have to be used to subtract the contribution of confounding factors such as vegetation, or to avoid confusion with other surface types such as dry sand. The following satellite observations were used to generate GIEMS: passive microwave from the Special Sensor Microwave Imager (SSM/I) measurements between 19 and 85 GHz; active microwave backscattering coefficients at 5.25 GHz from scatterometers; and visible and near-infrared reflectances and the derived Normalised Difference Vegetation Index (NDVI). The methodology is described in detail in Prigent *et al.*, (2001). Pre-processing is applied to the passive microwave observations to suppress the modulation by the surface temperature and by atmospheric effects. The inundated pixels are identified with an unsupervised classification algorithm that merges the three sets of satellite observations and a mixture model that quantifies the fractional inundation in each pixel. The method is globally applicable without any tuning for specific environments. The availability and reliability of the active microwave and the visible/near-infrared observations imposed some fine-tuning of the initial methodology (details are provided in Papa *et al.* (2010)).

Fifteen years of global monthly water surface extents 1993–2007 are available, on an equal-area grid of 0.25° × 0.25° at the Equator (each pixel covers 773 km^2) (https://lerma.obspm.fr/spip.php?article91&lang=en). Regional assessment of this database using Synthetic Aperture Radar (SAR) data indicates that the approach realistically captures wetland complexes, but can underestimate small wetlands comprising less than 10% fractional coverage of a grid cell (<80 km^2), or overestimate wetlands of more than 90% of fractional coverage because of its coarse spatial resolution.

The dataset has been extensively evaluated at the global scale (Prigent *et al.*, 2007; Papa *et al.*, 2010) and for a wide range of environments, including boreal and tropical regions. Specific works over the SSA region with GIEMS include studies by Pedinotti *et al.* (2012) and Aires *et al.* (2014).

2.2 | Rainfall and cloud data

For this study, we use rainfall estimates provided by the Climate Prediction Center Morphing method (CMORPH version 1: Joyce *et al.*, 2004). Three-hourly rainfall is estimated using a combination of passive microwave and thermal images. Microwave data from polar-orbiting satellites provide more accurate rainfall retrievals than cloud-top temperatures from thermal sensors on board geostationary satellites. However, the frequency of overpasses providing microwave data is inadequate for estimating 3-hourly or daily rainfall. The CMORPH product is created by "morphing" in space and time the rainfall rates from consecutive microwave images using half-hourly cloud-top temperatures. As with other similar gridded sub-daily products (e.g. TRMM-3B42, IMERG, PERSIANN), uncertainties in rainfall totals can be large, even at the monthly time-scale. In this study we are less interested in absolute rainfall totals than spatial differences in rainfall – for this reason we do not use the gauge-corrected CMORPH product. For the current work we use 16 years of CMORPH data, from 1998 to 2013.

Some current passive microwave algorithms suffer from systematic biases over inland water bodies (Tian and Peters-Lidard, 2007). They found that total rainfall is overestimated over water bodies due to frequent false detections of light rain. Caution is therefore required when using CMORPH (and similar products) to detect spatial rainfall structures in the vicinity of surface hydrological features. For example, Paiva *et al.* (2011) were able to demonstrate a marked decrease in rainfall over large Amazonian water bodies. In this case, the rainfall signal runs counter to the systematic bias reported by Tian and Peters-Lidard (2007), and moreover its diurnal cycle fits with our knowledge of Amazon river breezes (Silva Dias *et al.*, 2004). It is for this reason that we also exploit the alternative, and much more accurate, measurement of rainfall intensity provided by the precipitation radar on board the Tropical Rainfall Measurement Mission (TRMM). These data are independent of the measurements that are used to create CMORPH, but are only available typically once every 3 days. We use the surface rainfall rates from the TRMM2A25 product (available from https://disc.gsfc.nasa.gov/information) to create maps for comparison with our CMORPH data. In this way we can avoid drawing conclusions based on artefacts from the rainfall retrieval process. The data have a spatial resolution of 4–5 km, and are available for the period 1998–2013.

Finally, to examine different phases of the life cycle of convection, we analyse a multi-decadal dataset of half-hourly thermal infrared brightness temperature from the Meteosat First Generation series of satellites. The data are produced by the Meteosat Visible and Infrared Imager (MVIRI) from measurements in the range of 10.5–12.5 μm, at a resolution ~4.5 km at the Equator. Here we use data extracted from the EUMETSAT archive (https://www.eumetsat.int) for the months June–September from 1982 to 2005 over the Sahel, as used in a previous study (Taylor, 2010). We define MCS based on contiguous cold-cloud areas exceeding a threshold of 5,000 km^2, using a temperature threshold of −40 °C. These systems are responsible for the vast majority of rain in the Sahel, particularly when the systems are fast-moving (Mathon *et al.*, 2002), and during late afternoon and evening, when the systems are in their developing and mature phases (Futyan and Del Genio, 2007).

3 | TEMPORAL VARIABILITY IN WETLAND EXTENT

The major motivation for examining the impact of wetlands on rainfall is that wetlands are, by their nature, dynamic. Natural variations in rainfall (local or upstream) can therefore feed back on subsequent rain via perturbations in wetland fluxes into the atmosphere. Hence we begin our analysis by using the GIEMS dataset to identify the major wetlands in sub-Sahara Africa and characterize their temporal variability (Figure 1). Considering all African land grid points south of 17°N, ~22% contain wetland extent of at least 10% for at least 1 month in the 15-year time series. The wetlands with the greatest seasonal variation in extent (Figure 1a, monthly maximum minus minimum) are the Barotse (along the upper Zambesi river on the Angola/Zambia border), the Niger Inland Delta (or "Mali wetlands"), around Lake Bangweulu (in northern Zambia), around the confluence of the Chari and Logone rivers (on the Chad/Cameroon border), and the Okavango and Magadikadi wetlands in Botswana. Other extensive wetlands depicted in Figure 1a include the Sudd and Bar Al Ghazal wetlands (in South Sudan), and the Cuvette Centrale of the Congo Basin (in the Democratic Republic of Congo). Note that several major water bodies which exhibit marked seasonal and interannual variability in extent (including Lake Chad, to the north of the Chari/Logone wetland) are masked out in the GIEMS dataset.

The seasonality of these wetlands (Figure 1b) is driven primarily by the seasonal migration of the rains within the intertropical convergence zone (ITCZ). The Sahelian and Soudanian regions just to the south of the Sahara experience a single wet season during Northern Hemisphere summer, and this produces peak wetland extents at the end of the rainy season (typically October). Where the movement of water through the wetlands is very slow, the maximum wetland extent may lag local rainfall by many months. For example, the maximum wetland extent in the northernmost reaches of the Sudd is in January, 3–4 months after the end of the local rainy season. Across Southern Africa, maximum

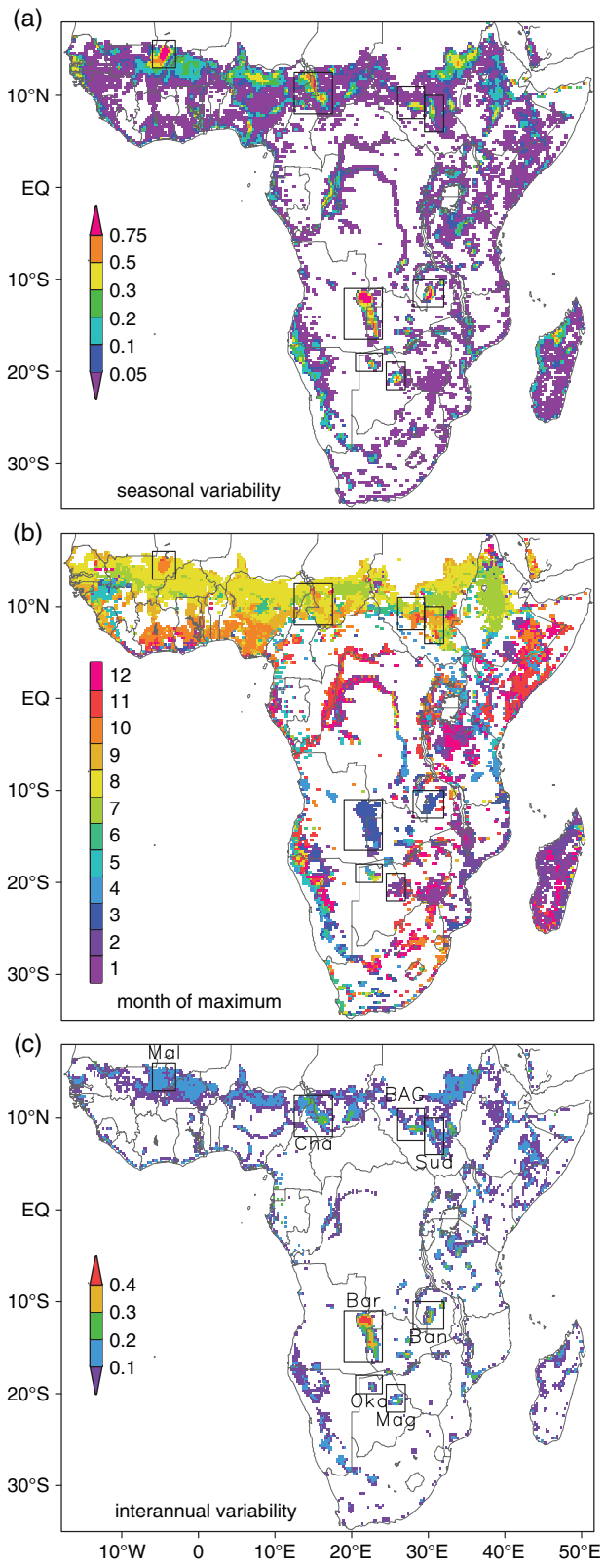

FIGURE 1 Wetland fraction characteristics in the GIEMS dataset computed from a seasonal climatology. (a) Monthly maximum minus minimum wetland fraction, (b) month of maximum wetland extent, and (c) interannual standard deviation of wetland extent for the month with the largest interannual variability. For clarity, pixels with standard deviations of less than 0.05 are masked out in (c). The following major wetlands are labelled; Mali (Mal), Chari/Logone (Cha), Bar Al Ghazal (BAG), Sudd (Sud), Barotse (Bar), Okavango (Oka), Bangweulu (Ban) and Magadikadi (Mag)

wetland extents occur predominantly during January to April, again in the latter stages of the local wet season. The Okavango provides a good example of a wetland fed largely by upstream rainfall, reaching a maximum extent in May, several months into the local dry season (Wolski *et al.*, 2006). The ITCZ crosses the moist tropical belt which straddles the Equator during both March–May and September–November. The combination of large catchments for some wetlands (notably in the Congo River basin) and these two wet seasons leads to Central African wetland maxima most frequently occurring in May/June and December/January.

Interannual variability in wetland extent is quantified in Figure 1c as the maximum monthly value of the interannual standard deviation. For the Northern Hemisphere wetlands, this coincides approximately with the month of maximum extent (i.e. at the end of the wet season). For the major Southern Hemisphere wetlands (Barotse, Okavango and Bangweulu), maximum interannual variability is found a month or two ahead of peak extent. In terms of magnitude, the upper parts of the Barotse wetland stand out as a clear maximum in this analysis, with standard deviations exceeding 0.3 during January and February. Other wetlands with strong interannual variations include the Lake Bangweulu region, the Magadikadi, and the wetlands of the Chari/Logone and Bar Al Ghazal.

4 | SPATIAL VARIABILITY OF RAINFALL IN THE VICINITY OF WETLANDS

Seeking to isolate the influence of land surface hydrology (e.g. wetland extent, soil moisture) on precipitation from observations is not straightforward. Local rainfall variability is the dominant driver of soil moisture and, at least for small catchments, wetlands. When one considers that in addition, the atmosphere can exhibit persistence which favours (or suppresses) rainfall on time-scales out to months in many tropical regions linked to oceanic forcing, it is difficult to interpret correlations between surface hydrological variables and subsequent rainfall as causation (Tuttle and Salvucci, 2016). On the other hand, looking instead at long-term spatial patterns in rainfall in the vicinity of a surface feature such as a wetland, if there is a significant local wetland forcing on rain, it should start to emerge in those patterns. It is important when doing such spatial analysis to minimise the influence of other fixed features of the landscape, notably strong variations in topographic height or proximity to coastlines (and associated sea breezes), both capable of triggering convection, and thereby introducing mesoscale structure into the long-term rainfall pattern.

In Figure 2 we present afternoon rainfall patterns around eight African wetlands. These wetlands are chosen (from Figure 1) on the basis of large spatial extent, strong temporal fluctuations, and relatively weak topographic or coastal variability. The afternoon period is chosen as this is when

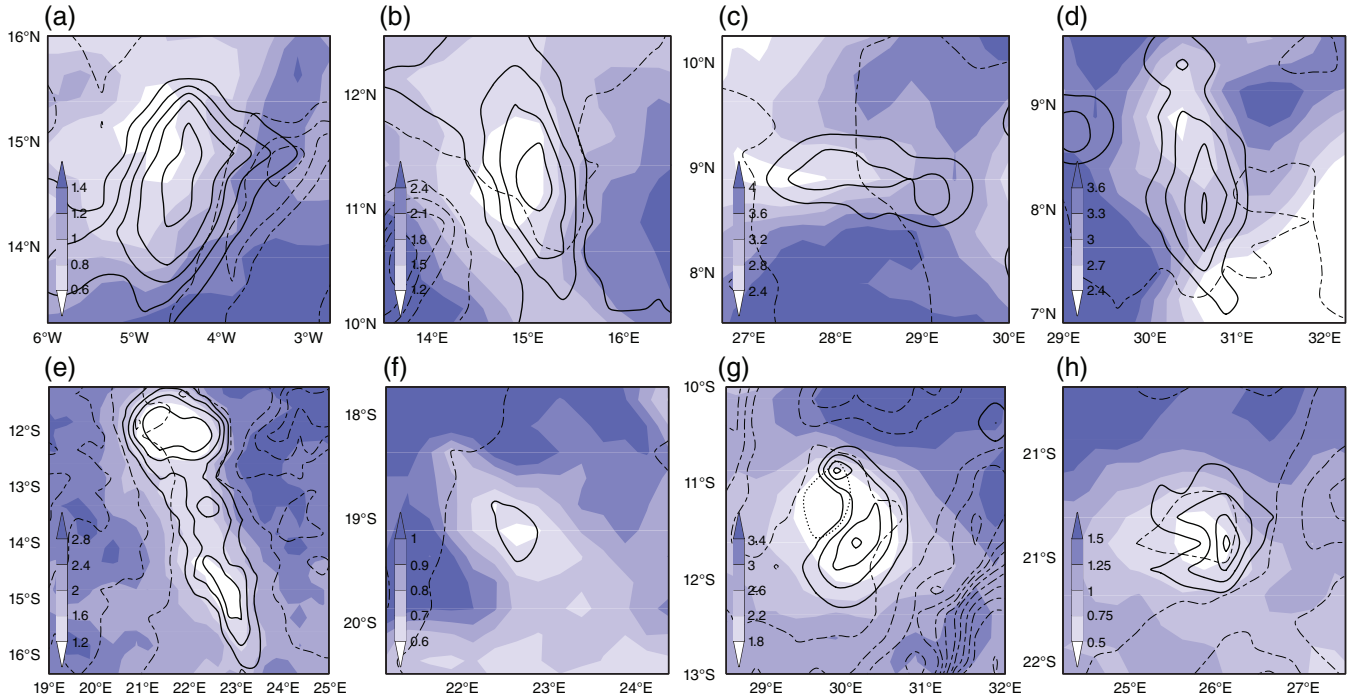

FIGURE 2 Mean afternoon rainfall accumulations from CMORPH (shading; mm) over major African wetlands for selected months. (a) Mali wetlands (September–October), (b) Chari/Logone wetlands (Cameroon/Chad, September/October), (c) Bar Al Ghazal (South Sudan, September–October), (d) Sudd (South Sudan, September–October), (e) Barotse (Zambia, February/March), (f) Okavango (Botswana, March–April), (g) Bangweulu (Zambia, January–February), and (h) Magadikadi (Botswana, February–March). Solid contour lines denote mean wetland fraction of 0.1, 0.3, 0.5, 0.7 and 0.9, whilst the dotted line in (g) indicates the permanent water body of Lake Bangweulu, which is not featured in the GIEMS dataset. Dot-dashed contours denote topographic height every 100 m. Rainfall is accumulated between 1200 and 1800 UTC, except for the Mali wetland, where an accumulation period of 1500–2100 UTC is chosen [Colour figure can be viewed at wileyonlinelibrary.com]

surface-induced impacts on the atmosphere are likely to be both strong (maximum development of the PBL, and favoured period of convective initiation), and also more spatially coherent with the surface. Once the sun goes down and surface fluxes become small, local surface-induced variations in the temperature and humidity in the lower atmosphere will mix out and be advected away from the surface forcing. The definition of "afternoon" in Figure 2 is two consecutive 3 h periods starting at either 1200 or 1500 UTC, depending on local time variations in East and West Africa. The rainfall data are averaged over the 2 months in the rainy season when, climatologically speaking, the wetland is at maximum extension. Note that the rainfall and wetland climatologies plotted in Figure 2 are constructed from different (though overlapping) periods; 1998–2013 in the case of rainfall, and 1993–2007 for the wetlands. We therefore assume that the impact on rainfall of any differences in mean wetland extent between these two overlapping periods is small compared to the impact of the long-term mean wetland extent. We explicitly consider interannual variability in wetland extent later.

In each of the panels shown in Figure 2, large-scale rainfall gradients are evident – for example, rapidly declining rainfall moving north in the two Sahelian wetlands (a, b). However, all eight wetlands exhibit locally suppressed rainfall patterns, either over (d to h), or slightly to the west (a to c) of the wetlands themselves. The coherence of the spatial patterns of wetland extent and rainfall is clearest for the Barotse (e), where mean afternoon rain accumulations range from less than 1.2 mm over the centre of the wetland to greater than 2 mm over the drier surroundings some 100 km away, equivalent to a drop in rain ~40% over the wetland itself. Based on Figure 2, estimated suppression of afternoon rain at the centre of the wetland (or in the case of Figure 2a–c, ~30 km to the west of the centre) lies in the range of 20% (for the Sudd, Figure 2d) to 60% (for the Magadikadi, Figure 2h). The largest wetland rainfall gradients (in absolute terms) are found for the Barotse (Figure 2e) and around Lake Bangweulu (Figure 2g). Qualitatively similar rainfall patterns to those shown in Figure 2 are also found in the alternative TRMM3B42 rainfall dataset (Huffman *et al.*, 2007), in spite of differences in mean rainfall at the larger scale.

Also shown in Figure 2 are contours of topographic height (every 100 m). By their nature, wetlands tend to occur in areas of locally low elevation. Therefore in regions where the presence of hills can preferentially trigger convection, one might obtain negative correlations between wetland fraction and afternoon rain purely as an artefact of this (non-hydrological) process. Considering the case of the Barotse (Figure 2e), there certainly is higher ground either side of the wetland in the northern part of the domain, and this may well play a role in determining local rainfall patterns. However, as the Zambesi flows south beyond 14°S, the surrounding landscape flattens out. With no significant topography here for over

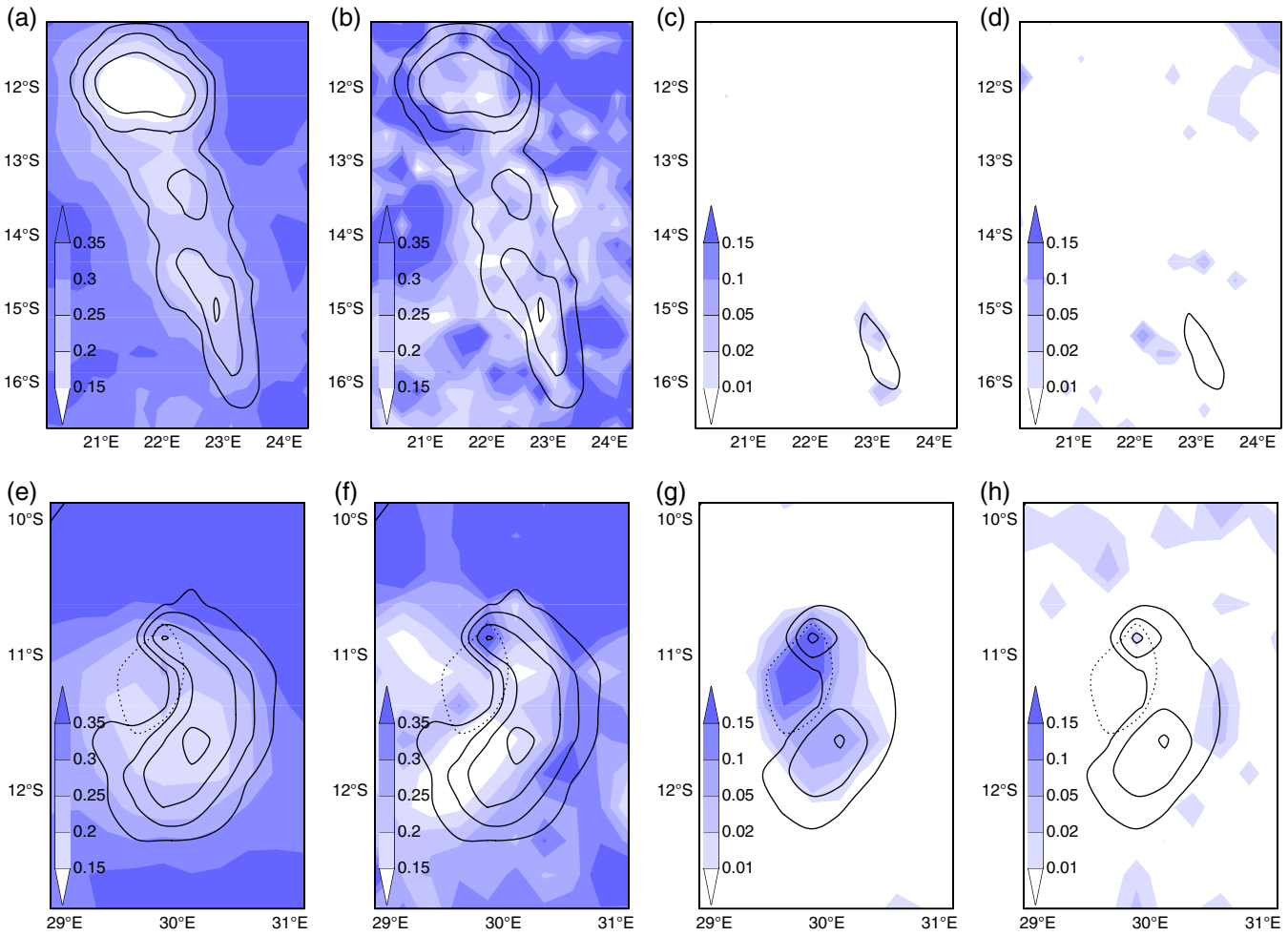

FIGURE 3 Comparison of mean afternoon (1200–1800 UTC) rainfall rate (shaded; mm/h) around the (a–d) Barotse and (e–h) Bangweulu wetlands based on (a,c,e,g) CMORPH and (b,d,f,h) TRMM PR data. The data in the first two columns are for the wet season months of January–April, whilst the last two columns are for the dry season months of May–August. The solid contours denote mean seasonal wetland fraction, and the dotted lines indicate the location of the permanent water body Lake Bangweulu [Colour figure can be viewed at wileyonlinelibrary.com]

150 km in any direction, it is difficult to invoke a purely topographic mechanism to explain the strong suppression of rain over the centre of wetland (around 15°S, 23°E). The potential role of topographic height around the Barotse will be further explored later.

The common feature of local minima in rainfall over the eight wetlands is consistent with previous independent analysis around the Mali wetlands (Taylor, 2010). That study made no use of CMORPH rainfall, and only used the GIEMS data to evaluate a thermal remote-sensing approach to wetland estimation. Figure 2 is also consistent with observational studies of soil moisture effects on afternoon rain (Taylor and Ellis, 2006 Taylor *et al.*, 2011; 2012). Those studies all show that in the absence of pre-existing propagating convective systems, afternoon rain is enhanced over drier surfaces (with lower evapotranspiration and higher sensible heat flux) compared to nearby wetter surfaces. This all points towards an important role for surface fluxes in perturbing rainfall around African wetlands. On the other hand, the common, and indeed striking, rainfall signal surrounding all eight major wetlands in Figure 2 could be the result of systematic biases in passive microwave-derived rainfall estimates (CMORPH) in the vicinity of wetlands, as discussed in the introduction. To verify that the CMORPH data are not subject to contamination from the wetland data, a comparison is made between the regular 3-hourly CMORPH estimates and data from the TRMM precipitation radar for the two wetlands with the strongest (in absolute terms) rainfall signals, the Barotse and Bangweulu. The radar data have been interpolated onto the same regular 0.25° grid as CMORPH, with each grid cell comprising mean surface rainfall estimates from between 172 and 182 overpasses during the period 1998–2014 for selected periods of the day and year. The temporal sampling of the two datasets is totally different, resulting in a much more speckled "average" afternoon rainfall map from TRMM than found from CMORPH (Figure 3). Notwithstanding this, broadly similar spatial structures are retrieved from the two datasets, with rain suppressed over the wetlands during the wet season in both. We therefore conclude that any potential surface contamination issues with CMORPH are not responsible for the observed wetland signal during the wet season.

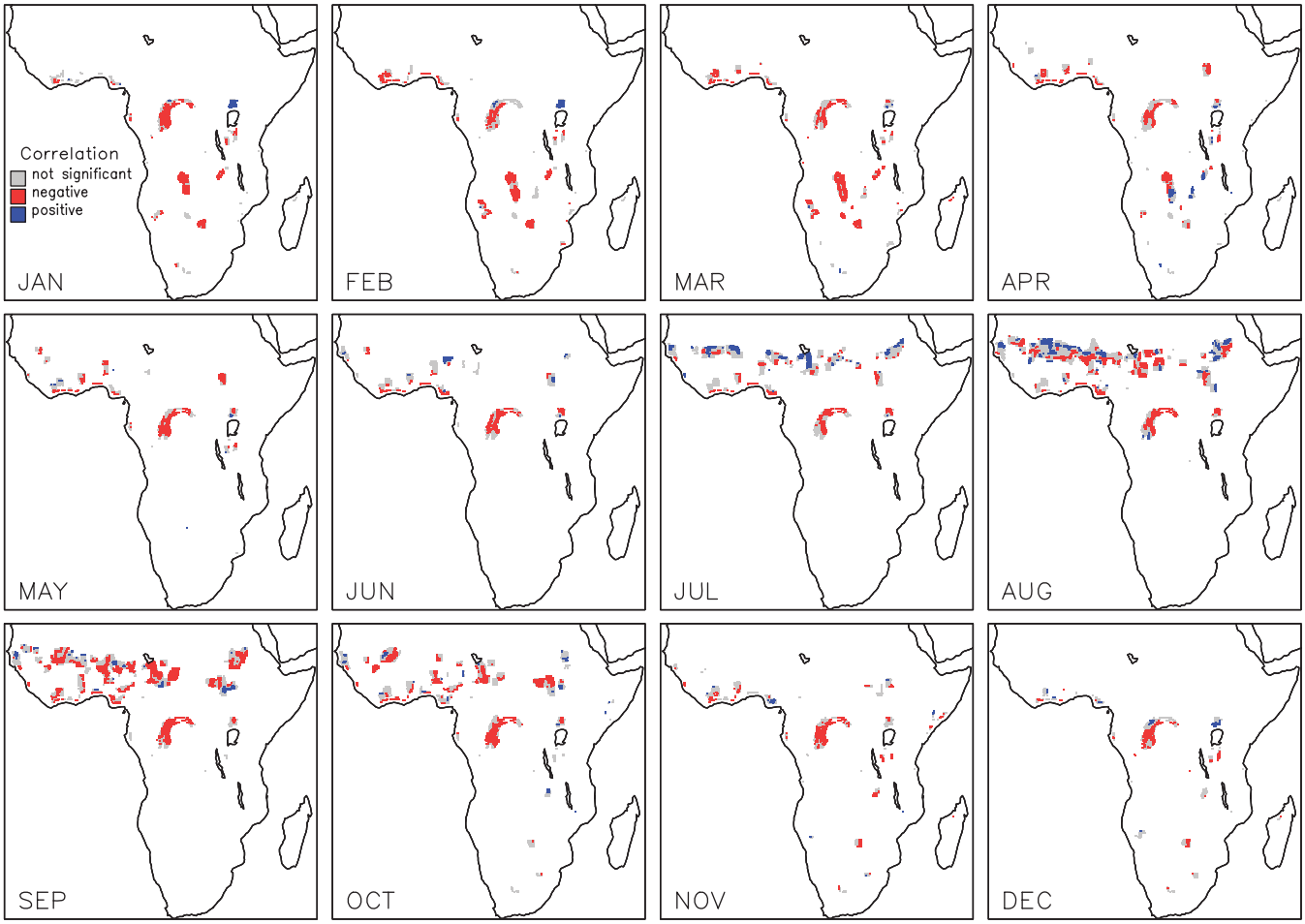

FIGURE 4 Monthly maps of spatial correlations between afternoon rainfall accumulations and wetland fraction. Blue (red) shading denotes pixels with a significant positive (negative) correlation at the 95% level according to a two-tailed test. Grey shading indicates no significant correlation, whilst white areas show where no correlation test was performed, due to either lack of wetland, or presence of topography or coastline

The comparison with TRMM radar data is repeated during the dry season, when CMORPH depicts spatially coherent but small-amplitude rainfall structures of the opposite sign (i.e. rain over the wetland) for these two wetlands. In the case of Lake Bangweulu, a mean afternoon accumulation of 0.1 mm is detected over the lake and surrounding wetland from CMORPH. Whilst this rainfall is very small, and in terms of a single event, well below the quoted accuracy of the product, similar features are found during the dry season over other wetlands. These features stand out compared to accumulations of effectively zero from the surroundings. The TRMM precipitation radar provides no supporting evidence for this apparent positive feedback. Moreover, inspection of time series of dry season cloud-top temperature data around Lake Chad (not shown) also brings into question the dry season rain signal apparent in CMORPH. Indeed, according to CMORPH, in several pixels within Lake Chad there is rainfall greater than 0.1 mm in 40–50% of the 3-hourly estimates during the intensely dry month of March. Taken together, these pieces of evidence strongly suggest that during the dry season, spatial patterns in rainfall from CMORPH around African wetlands and open water are not reliable. It is likely they suffer from the same bias previously found from water bodies in the United States (Tian and Peters-Lidard, 2007). During the wet season, either these biases are not present, or are considerably smaller than the actual (reverse) rainfall gradient, as concluded by Paiva *et al.* (2011) over large Amazonian rivers.

We now put the above analysis on a more quantitative footing for all sub-Saharan wetland areas and all phases of the diurnal and seasonal cycles. Local spatial correlations of climatological wetland fraction and CMORPH rainfall are computed for all land points, for every month of the year, and for each of the eight 3 h periods over which rainfall is estimated. The spatial correlation for a particular 0.25° grid point is determined from a linear regression between wetland fraction and rainfall for the 25 grid points within a "local" box of length 1.25° × 1.25° centred on the grid point in question. The analysis is not performed if the local box is deemed to contain strong topographic forcing. Following Taylor *et al.* (2012), we use a threshold of 300 m, which defines the maximum permissible range of surface heights within the local box using the ETOPO1 topography dataset at 1 arc-minute spatial resolution (https://www.ngdc.noaa.gov/mgg/global/global.html). We also exclude local boxes which include sea points (i.e. less than or equal to 0 m topographic height). To minimise the

effects of wetland detection errors at low extents on the analysis, we impose a minimum wetland fraction within the 25 local box grid points of 0.1. Finally, we only compute correlations when average rainfall exceeds 0.01 mm/h throughout the local box, to filter out the weak systematic dry season biases in CMORPH rainfall found over water bodies (discussed above).

The results of the spatial correlation analysis are presented in map form in Figure 4 for every month in the year, for rainfall accumulations between 1500 and 1800 UTC. Red (blue) shading indicates a negative (positive) local correlation between rainfall and wetland extent, which is significant at the 95% level (according to a two-tailed Student's *t*-test), whilst grey indicates locations where correlations have been computed, but the regression gradients are not significantly different from 0 at the 95% level. White indicates either no wetlands, insufficient rain, or the presence of topographic variability or coastlines. What is immediately evident is the dominance in every month of negative (red) correlations over positive (blue). This is entirely consistent with the qualitative maps of afternoon rainfall around major wetlands in Figure 2. Interestingly, Figure 4 shows significant negative correlations in moist tropical regions (i.e. the Congo Basin) as well as semi-arid zones to the north and south. Note that repeating these calculations only considering rainfall rates greater than 5 mm/h produces almost identical maps as in Figure 4.

To quantify the dominance of this effect, Figure 5 presents the percentage of grid cells for which regressions were performed, which have significant negative correlations. These are shown as a function of month of year and time of day, and illustrate a very clear diurnal cycle peaking during the afternoon. Indeed for the period 1200–1800 UTC, this percentage exceeds 30% in all months except July. Overnight, and in particular in the hours before sunrise (0300–0600 UTC), the fraction of grid cells with negative correlations falls to 10–20%. Similar analysis of the fraction of grid cells with significant positive correlations (i.e. the fraction of blue pixels compared to all coloured pixels in Figure 4) shows no such strong features. The largest occurrence of pixels contributing positive correlations is between 0300 and 0600 UTC, but this only reaches 10–20%, a similar proportion to negative correlations at this time of day.

In the above statistical analysis, we have neglected the effects of spatial autocorrelation. In fact the climatological rainfall distribution across the 5×5 grid cells used in each calculation is likely to be influenced by large-scale rainfall gradients, particularly on the poleward fringes of the ITCZ (for example the Sahel during northern summer). This can result in paired areas of significant positive and negative correlations which affect the overall (pan-African) statistics. Good examples of this paired behaviour are found in July and August across Mali, Burkina Faso and northern Nigeria (Figure 4). To the south of those wetlands the rainfall increases, driven primarily by the large-scale gradient. This effect favours a negative correlation (on top of any local wetland impact), whilst the opposite occurs on the

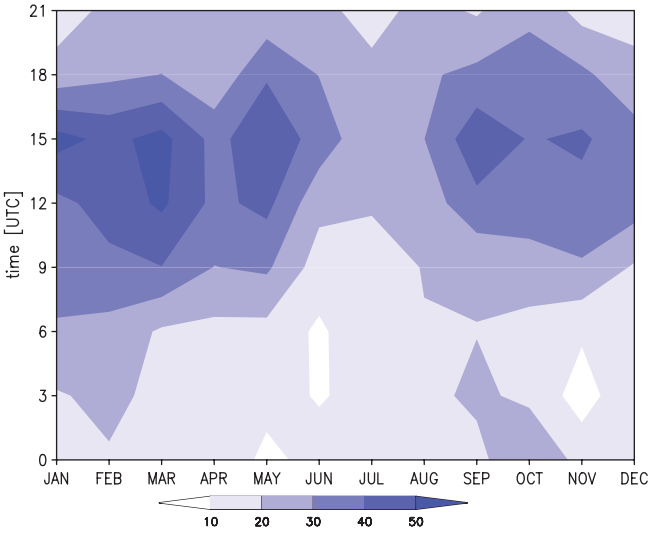

FIGURE 5 Percentage of pixels in the vicinity of sub-Saharan African wetlands with significant negative correlations between rainfall and wetland fraction. The correlations are computed for each 3 h time of day for which CMORPH data are available, and for each month of the year [Colour figure can be viewed at wileyonlinelibrary.com]

northern side of many Sahelian wetlands, favouring positive correlations. On average, these pairings cancel out, though neglecting this autocorrelation does increase the frequency of significant values compared to an expectation of 2.5% for each from a 2-tailed 95% significance test.

We now consider an alternative hypothesis explaining the predominantly negative correlations between afternoon rainfall and wetland fraction, namely the potential influence of fixed topographic features. We examine interannual variability in rainfall patterns to assess whether the signal of locally suppressed rain over a wetland is stronger (weaker) in periods when wetland extent is large (small). We analysed rainfall between 1200 and 1800 UTC for each of the wetlands highlighted in Figure 2. The two datasets have only 10 years in common (1998–2007), and within these, we only considered the two wet-season months (shown in Figure 2a) when wetland variability is strong. For each of the wetlands, we ranked the 20 remaining monthly values of total wetland extent to identify the 5 largest and 5 smallest wetland extents (i.e. the first and fourth quartile). We used these two sets to construct composite mean datasets representative of large and small extents.

Results of the composite analysis are shown in Figure 6 for the three cases with the strongest interannual variability in extent – the Barotse, Bangweulu and Magadikadi wetlands. It should first be noted that as rainfall (both local and upstream) drives wetland extent, one might expect more rain during months with extensive wetland, a mechanism that requires no feedback of the surface on the atmosphere. It turns out that in two of these three cases, for the sets of months used for compositing, less rain falls directly over the wetlands when extents are large (i.e. negative differences in Figure 6a,b). This is not the case for the Magadikadi (Figure 6c), where the greatest wetland extents during February and March coincide with

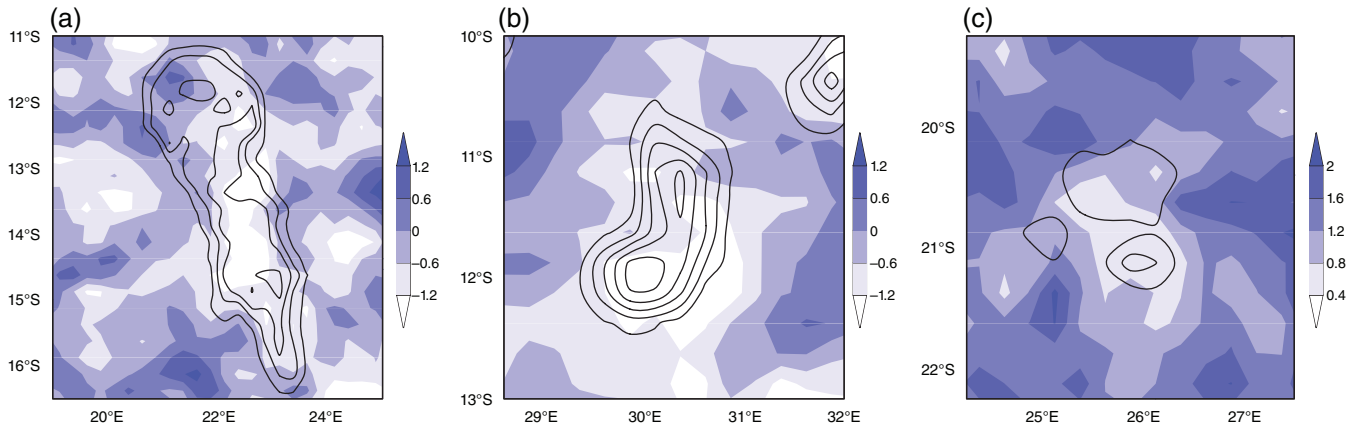

FIGURE 6 Differences in CMORPH afternoon (1200–1800 UTC) rainfall accumulations (shading; mm) and wetland fractions (contours at 0.1, 0.3, 0.5 and 0.7) between wet season months with large and small wetland extent. Data are shown for the (a) Barotse, (b) Bangweulu and (c) Magadikadi wetlands. The composites are based on upper and lower quartiles of wetland fraction for the months of February and March (January and February in the case of the Bangweulu wetland) drawn from the years 1998–2007 [Colour figure can be viewed at wileyonlinelibrary.com]

larger regional rainfall. Nonetheless, though the rainfall differences between the composites in Figure 6 are somewhat noisy, based as they are on only 10 months of data, all three clearly exhibit suppressed afternoon rain (pale shading) over the areas of enhanced wetland (solid contours) in comparison to the surrounding areas. When analysed in this way, the other wetlands also exhibit local rainfall suppression over the wetland, though the signal is weaker (not shown). The weaker signals in those cases are likely related to their relatively modest interannual differences in wetland extent. The results of this temporal compositing, consistent with similar previous analysis for the Mali wetlands (Taylor, 2010), provides further evidence that variations in wetland extent influence local rainfall patterns. In the next section we analyse the impact of wetlands on rainfall at two key phases in the convective life cycle.

5 | IMPACT OF WETLANDS ON LIFE CYCLE OF CONVECTION

We now use higher spatial and temporal resolution cloud-top temperature data to examine the influence of two wetland areas within the West Africa monsoon region on the initiation and propagation of MCS. Previous work using this dataset identified clear impacts of the Mali wetlands (Taylor, 2010) on these key aspects of MCS life cycle, and here we complement that analysis with a focus on the wetlands surrounding the Chari and Logone rivers in the border region of Chad, Cameroon and Nigeria, and the Lake Chad area further north. The Chari/Logone wetlands occur on the southern fringes of the Sahel, where seasonal (June–September) mean rainfall averages ∼9 mm/day according to CMORPH. This compares with mean rainfall ∼ 5 mm/day in the region of Lake Chad (similar to conditions around the Mali wetlands). As a result of increased rainfall further south, there are likely to be weaker sensible heat fluxes in the dryland areas surrounding the Chari/Logone wetlands compared to the more water-stressed Sahelian conditions around Lake Chad.

The map in Figure 7 depicts the percentage of wet season days for which small to medium-sized (5,000–20,000 km^2) MCS have been detected at 1600 UTC. This subset of MCS is selected to filter out the largest systems, which tend to have been initiated many hours before, at locations well to the east. Figure 7 therefore indicates areas of preferential local triggering of MCS during the afternoon. The dominant feature in Figure 7a is a pronounced maximum in convective activity over and to the west of the Mandara mountains (marked "M"). Further notable local maxima in MCS activity are evident directly to the north of the mountains on the western side of the wetlands, by the northern tip of Lake Chad, and to a lesser extent, on its western and southern shores. Over the centre of Lake Chad there is a minimum in MCS at 1600 UTC. From examination of cold-cloud frequency maps in the preceding hours, the local maxima all appear as spatially distinct favoured locations for the development of MCS. The Mandara mountains, rising more than 500 m above the plains, are evidently an important trigger for convective initiation. The analysis here indicates that areas surrounding the wetlands also provide favourable conditions for convective initiation and development of MCS. This supports the conclusion drawn in the previous section that afternoon rainfall maxima around wetlands are due primarily to locally initiated convection. As with the earlier study from the Mali wetlands, there is a weak preference for convective initiation on the upwind rather than downwind side of the wetlands (in this case upwind is to the southwest) but accompanied (in the case of Lake Chad) by a notable maximum on the northwestern shore, perpendicular to the low-level southwesterly wind. The suppression of initiation over and downwind of wetlands is consistent with previous observational studies of convective initiation in areas of mesoscale soil-moisture heterogeneity (Taylor *et al.*, 2011; 2015). Numerical modelling studies (Taylor *et al.*, 2013Froidevaux *et al.*, 2014) show that landscape-induced daytime circulations, in combination with

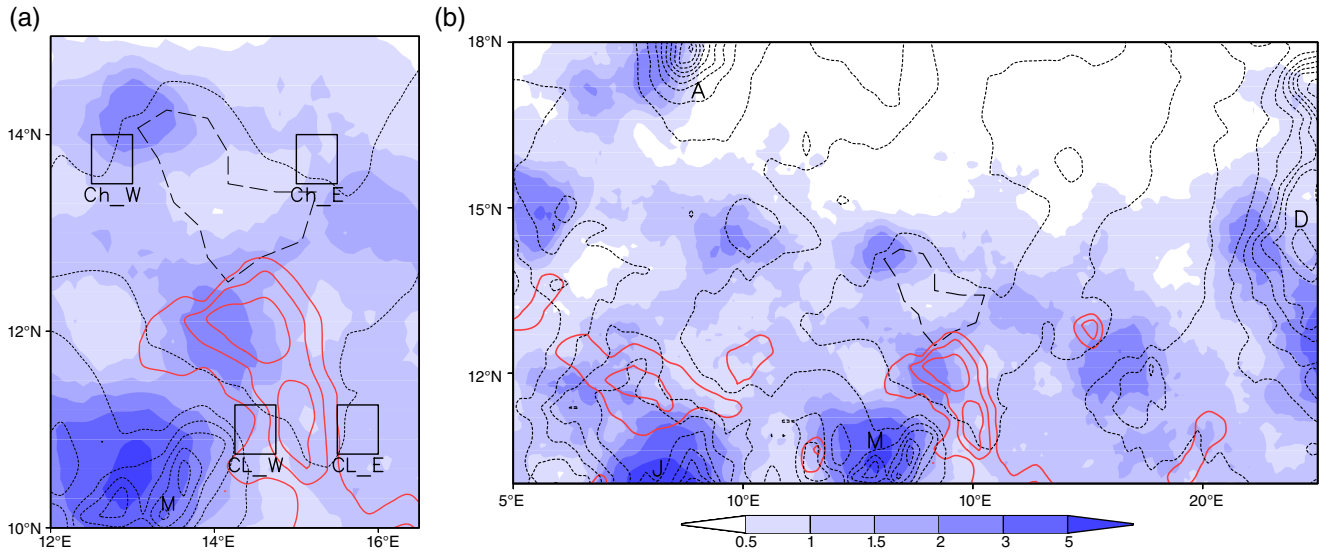

FIGURE 7 (a,b) Percentage of days (shading) with MCS between 500 and 20,000 km^2 at 1600 UTC for June–September (JJAS) 1982–2005. JJAS mean wetland fraction from the GIEMS dataset is depicted by solid red contours at 0.1, 0.2 and 0.3, whilst the outline of Lake Chad is indicated with long dashed contours. Topographic contours every 100 m are shown by short dashed lines. The locations of the mountains of Mandara, Darfur, Aïr and the Jos Plateau are marked with M, D, A and J respectively, and the compositing boxes west ("_W") and east ("_E") of Lake Chad ("Ch") and the Chari/Logone wetlands ("CL") are shown in (a) [Colour figure can be viewed at wileyonlinelibrary.com]

a weak large-scale wind, produce maximum convergence on the upwind edge of a wet surface feature.

To place these features in a broader geographical context, small to medium-sized MCS frequency is presented in Figure 7b over a much larger region. This highlights the importance for the initiation of MCS of the mountains of Darfur (on the Chad/Sudan border), the Aïr in northern Niger, and the Jos plateau in central northern Nigeria, as found in previous studies (Rowell and Milford, 1993). However, it also illustrates that in the context of the Sahel region (broadly speaking, north of 11°N in this region), the wetlands of the Chari/Logone rivers, and Lake Chad in particular, provide significant fixed triggers for MCS initiation. Whilst the frequency of a particular pixel containing a small to medium-sized MCS is only 2–3% in favoured locations around the wetlands (as compared to ∼5% for Darfur), it is at least double the frequency found elsewhere on the plains of the Sahel. In those locations lacking fixed convective triggers, transient soil-moisture patterns created by antecedent rain become important for the dominant land-surface mechanism for initiating convective storms (Taylor *et al.*, 2011).

We now examine the impact of these wetlands on the propagation of MCS of all sizes. To do this we identify, for a given time, all days in the dataset when an MCS is present within a box of length 0.5° either to the east (upstream in the sense of propagation of Sahelian MCS, controlled by the African Easterly Jet at 600–700 hPa) or west (downstream) of the wetland. The locations of these boxes are shown in Figure 7a. This allows us to create a composite MCS, defined in terms of its presence in the box at a particular time of day. Figure 8 presents the results of this analysis in terms of a Hovmüller (time–longitude) plot for each of the four boxes either side of Lake Chad (at 13.5–14°N), and the Chari/Logone wetlands (at 10.75–11.25°N), based on a compositing time of 1600 UTC. By definition, the maximum MCS frequency per pixel occurs within the box at 1600 UTC. In the composites, the maximum mean MCS areal coverage is ∼55%, indicating that many detected MCS do not extend across the entirety of the 0.5 × 0.5° box. The plots depict well-organised cold-cloud systems with a typical MCS westward propagation speed ∼14 m/s either side of 1600 UTC. Many of the systems detected to the west of Lake Chad (Figure 8a) are still captured in the composite 6 h later (i.e. 2200 UTC), with fractional coverage 300 km to the west of 39.8%. On the other hand, the composite based on systems to the east of Lake Chad (Figure 8b) loses coherence and weakens markedly when it reaches the longitude of Lake Chad (typically at 1730 UTC). Six hours after the compositing time, fractional coverage of MCS 300 km to the west of its origin is 29.6%, i.e. 10% lower than its western counterpart. Although the two composites are made up of similar numbers of cases (499 to the west and 456 to the east, of which 200 cases occur on the same days), they differ in terms of size distributions at the compositing time. West of Lake Chad (Figure 8a), high values of MCS coverage are more localised in longitude than to the east. This is consistent with there being a larger proportion of smaller, more rapidly developing systems to the west of Lake Chad, as depicted in Figure 7a for systems of between 5,000 and 20,000 km^2. Qualitatively similar features are found for the more southerly pair of composite MCS (Figure 8c,d). More MCS identified to the west of the Chari/Logone wetlands tend to have initiated locally, though the presence of the nearby Mandara mountains (around 13.8°E) is an important contributing factor here. As with the Lake Chad case, MCS detected on the western side of the wetlands tend to propagate further than those detected to the east, though the weakening

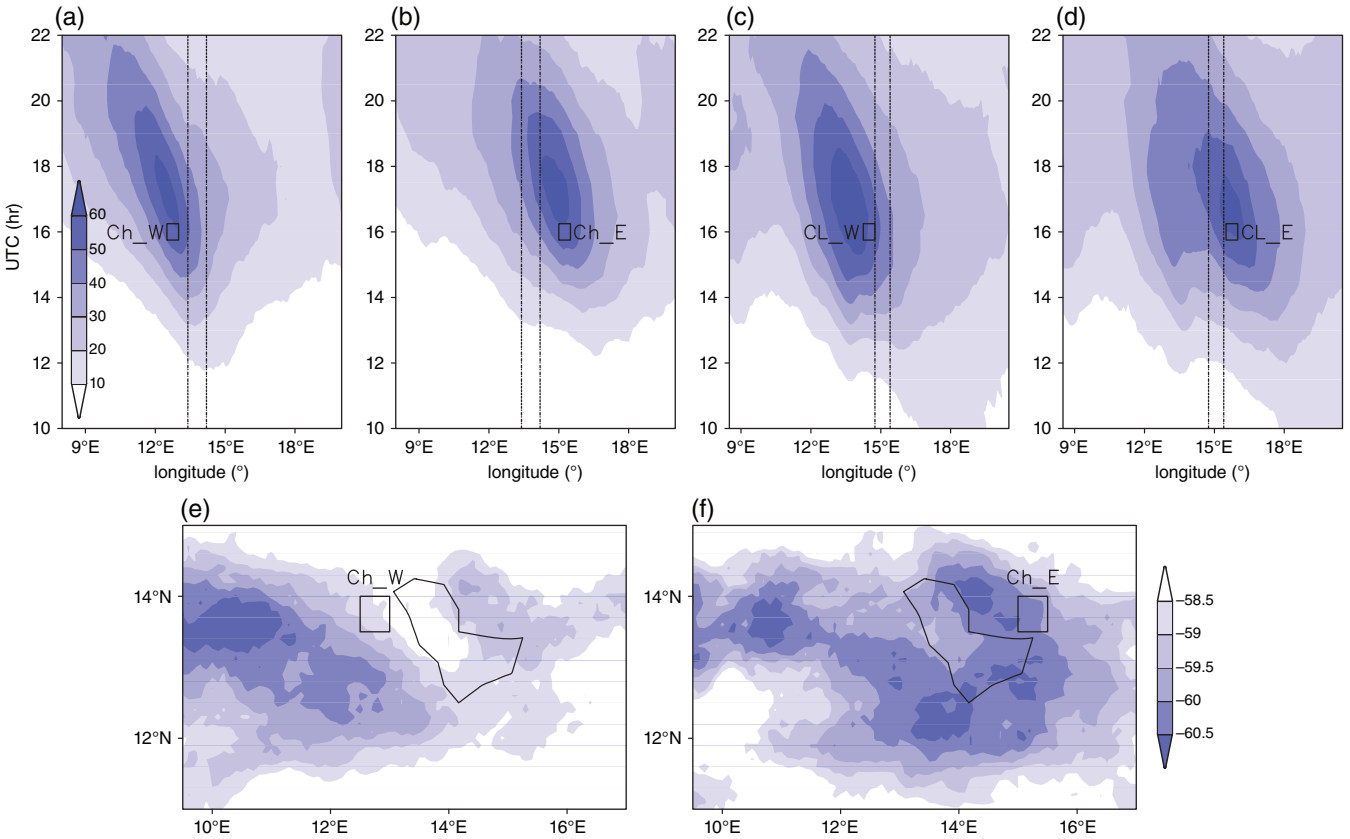

FIGURE 8 Evolution of composite MCS cloud fraction to the (a) west and (b) east of Lake Chad, and to the west (c) and (d) east of the Chari/Logone wetlands. Cloud fractions are based on averages between 13.5 and 14.0°N for Lake Chad, and 10.75 and 11.25°N for the Chari/Logone region. The vertical lines depict the approximate longitudinal extent of the wetlands at these latitudes, and the box indicates the time and longitude around which the MCS are composited. (e,f) The mean brightness temperatures (°C) for MCS pixels ($T < -40$ °C) between 1500 and 2200 UTC in the vicinity of Lake Chad based on the western and eastern composites respectively [Colour figure can be viewed at wileyonlinelibrary.com]

of the eastern composite MCS on reaching the Chari/Logone wetlands is less marked than for the Lake Chad case.

Alternative locations for the compositing boxes were also tested, with similar results. The composite analysis was also repeated with a compositing time of 0000 UTC to assess whether there may be a diurnal variation in the impact of the wetland on MCS propagation. However, rather similar weakening was detected for these overnight MCS approaching the two wetlands as for the afternoon systems depicted in Figure 8.

Finally, for the two Lake Chad composites, we show mean cloud-top temperatures computed from all pixels within an MCS, averaged between 1500 and 2200 UTC (Figure 8e,f). In the Sahel, this measure provides an indication of convective intensity (Taylor *et al.*, 2017). Both maps clearly depict coherent structures over the lake itself (amplitudes $\sim +1$ °C), consistent with decreasing MCS intensity as one moves west across the lake. Considering cold-cloud frequency and temperature composites together provides strong observational evidence to support the modelling study of Lauwaet *et al.* (2012). That analysis illustrated how the cold pool running ahead of the MCS weakened over the water body, leading to lower rainfall over the western side of the lake. They also found intensified convection within an MCS approaching the eastern shore, due to the plume of moist air which stretched northwestwards from the lake. It is difficult to say anything about the latter mechanism from these observations, although one can speculate that the slowing of the cold pool over the lake may produce longer-lived convective rainfall to the east of the lake.

On the other hand, the study by Lauwaet *et al.* (2012) reported no significant impact of the wetland breeze on precipitation. In their numerical model, the presence of Lake Chad more than doubled rainfall over the centre and eastern side of the lake. Those results are inconsistent with our analysis of convective initiation (Figure 7a), and CMORPH rainfall estimates (Figure 9). The two observational datasets show that over the centre and the eastern side of the lake there is in fact marked afternoon suppression of convection, which we assume is due to a wetland breeze. The mismatch between model and observations hints at an overly weak link between mesoscale circulations induced by landscape variability and convection in their simulations, consistent with many regional models with parametrized convection (Taylor *et al.*, 2013). Considering the full diurnal cycle (Figure 9b), CMORPH indicates lower rainfall overall on the lake compared to the same latitude further east or west, though the local minimum is extended to the west of the lake. This suggests that when considering the impact of Lake Chad on total rainfall, the contribution of enhanced afternoon convective

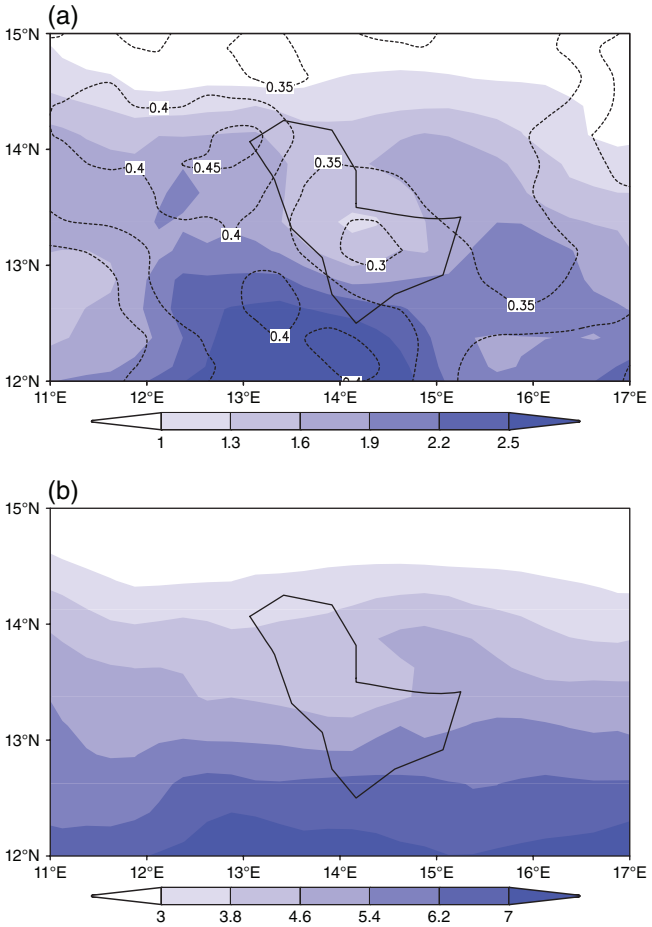

FIGURE 9 Mean rainfall (shaded; mm) in the vicinity of Lake Chad from CMORPH for JJAS accumulated over (a) the afternoon (1200–1800 UTC), and (b) the entire day. Dashed contours in (a) indicate the fractional contribution of afternoon rain to the daily total [Colour figure can be viewed at wileyonlinelibrary.com]

initiation to the west of the lake is more than offset by the weakening of westward-propagating MCS over the lake itself. This is likely linked to the high proportion of rain associated with mature MCS in the Sahel (Mathon *et al.*, 2002). In regions of Africa where MCS are less important contributors to total rain, we might expect a different balance between wetland effects on initiation and propagation of rainfall.

6 | CONCLUSIONS

Our analysis of satellite data around the major wetlands of SSA has revealed some common features in local rainfall patterns. Each of these wetlands was selected to avoid strong topographic influences on rainfall, which would make it more difficult to isolate potential impacts of the wetland on rainfall. Consistent across all the areas studied, we found suppression of rain over wetlands relative to adjacent drylands. Using local spatial correlation analysis, we found that across SSA, there is a strong diurnal signal, with negative rainfall anomalies over wetlands maximised during the afternoon. Indeed for 11 months in the year, at least 30% of pixels tested yielded negative correlations between afternoon rain and wetland fraction. This figure rises to 45% during the Southern Hemisphere wet season. Between 0000 and 0600 UTC on the other hand, this percentage tends to lie in the range 10–20%. Comparing rain over wetlands which exhibit strong interannual wet-season variability, we find afternoon rainfall gradients strengthen when wetlands are more extensive. Together, these analyses provide strong evidence that wetlands influence local rainfall across all major SSA wetlands studied.

We used higher space and time resolution cloud-top temperature data to identify the impact of Lake Chad and surrounding Chari/Logone wetlands on the life cycle of MCS. We found enhanced afternoon initiation of MCS around the wetland edges, accompanied by suppressed MCS activity over, and on the downwind side of the wetlands, as found in an earlier observational study (Taylor, 2010). In favoured locations close to these wetlands, afternoon MCS are twice as likely to develop as over dryland Sahelian plains at similar latitudes. Once triggered, MCS can influence rain several hundred kilometres away. Considering mature, remotely triggered MCS, the observations from Lake Chad and the Chari wetlands reveal a tendency for systems to weaken on reaching the wetland, consistent with a previous modelling study (Lauwaet *et al.*, 2012). The Sahel is characterised by contrasting wind directions at low level (southwesterly), and mid-(MCS steering-) level (easterly). The impact of the wetland on total rainfall locally is likely a combination of an MCS initiation feedback (suppressing rain over and to the northeast), and an MCS propagation feedback (suppressing rain over and to the west). More generally we might expect the net effect of the two feedback processes on wetland rainfall across Africa to depend on the balance between locally and remotely triggered convection. In the Sahel, the dominance of long-lived westward-propagating MCS on rainfall totals tips this balance towards a westward shift ~30 km in the rainfall minimum over the wetland. Elsewhere, the local rainfall minimum is essentially centred over the wetland.

The study provides evidence of favoured afternoon initiation of convection close to, but not over, wetlands, consistent with previous observational studies. Though not explicitly observed here, the likely mechanism is mesoscale circulations generated by the contrast in sensible heat between wet and drylands. Indeed, convection-permitting simulations have previously illustrated the importance of such landscape-induced circulations in a variety of environments (Rochetin *et al.*, 2017). Interestingly, we see this effect across all wetlands studied, from semi-arid cases (e.g. the Okavango), to deep within the tropical forest (wetlands surrounding the Congo River). This evidence for wetland influence is counter to some studies (Mohamed *et al.*, 2005), which argued that the contrast between fluxes was not big enough in the relatively moist climate of the Sudd. Instead we find a negative precipitation–wetland extent correlation around the Sudd dominates for many months of the year.

This study illustrates the influence of wetlands on rainfall both locally and regionally. Wetlands respond to both climatic

variability and changes in upstream water use. Consideration should be given to the impacts of major river management schemes on downstream rainfall via changes in wetland seasonality and extent. For example, plans to construct a large reservoir for water supply, hydropower and irrigation at Fomi, Guinea are likely to reduce and attenuate seasonal flooding of the Niger Inland Delta (Liersch *et al.*, 2013) with potential effects on rainfall in the western Sahel. Changes in MCS-induced precipitation might also be included in assessments of the impact of potential water diversions such as drainage of the Bahr el Ghazal swamps (Eltahir, 1989) and the construction of the Jonglei Canal in the Sudd (Mohamed *et al.*, 2005). Equally, this study suggests that continued reductions in the extent of Lake Chad and its associated wetlands may influence rainfall to the west via changes in the population of MCS.

ORCID

Christopher M. Taylor https://orcid.org/0000-0002-0120-3198

REFERENCES

Acreman, M. and Holden, J. (2013) How wetlands affect floods. *Wetlands*, 33, 773–786. https://doi.org/10.1007/s13157-013-0473-2.

Aires, F., Papa, F., Prigent, C., Crétaux, J.-F. and Berge-Nguyen, M. (2014) Characterization and space–time downscaling of the inundation extent over the inner Niger Delta using GIEMS and MODIS data. *Journal of Hydrometeorology*, 15, 171–192. https://doi.org/10.1175/jhm-d-13-032.1.

Alter, R.E., Im, E.-S. and Eltahir, E.A.B. (2015) Rainfall consistently enhanced around the Gezira scheme in East Africa due to irrigation. *Nature Geoscience*, 8, 763–767. https://doi.org/10.1038/ngeo2514.

Coe, M.T. and Foley, J.A. (2001) Human and natural impacts on the water resources of the Lake Chad basin. *Journal of Geophysical Research: Atmospheres*, 106, 3349–3356. https://doi.org/10.1029/2000JD900587.

Dadson, S.J., Hall, J.W., Murgatroyd, A., Acreman, M., Bates, P., Beven, K., Heathwaite, L., Holden, J., Holman, I.P., Lane, S.N., O'Connell, E., Penning-Rowsell, E., Reynard, N., Sear, D., Thorne, C. and Wilby, R. (2017) A restatement of the natural science evidence concerning catchment-based 'natural' flood management in the UK. *Proceedings of the Royal Society A: Mathematical, Physical and Engineering Science*, 473, 20160706. https://doi.org/10.1098/rspa.2016.0706.

Denman, K.L., Brasseur, G., Chidthaisong, A., Ciais, P., Cox, P.M., Dickinson, R.E., Hauglustaine, D., Heinze, C., Holland, E., Jacob, D., Lohmann, U., Ramachandran, S., Dias, P.L.S., Wofsy, S.C. and Zhang, X. (2007) Couplings between changes in the climate system and biogeochemistry. In: Solomon, S., Qin, D., Manning, M., Chen, Z., Marquis, M., Averyt, K.B., Tignor, M. and Miller, H.L. (Eds.) *Climate change 2007: The physical science basis. Contribution of Working Group I to the fourth assessment report of the Intergovernmental Panel on Climate Change*. Cambridge: Cambridge University Press, pp. 501–568.

De Ridder, K. (1997) Land surface processes and the potential for convective precipitation. *Journal of Geophysical Research: Atmospheres*, 102, 30085–30090.

Eltahir, E.A.B. (1989) A feedback mechanism in annual rainfall, Central Sudan. *Journal of Hydrology*, 110, 323–334. https://doi.org/10.1016/0022-1694(89)90195-9.

Findell, K.L. and Eltahir, E.A.B. (2003) Atmospheric controls on soil moisture–boundary layer interactions. Part I: Framework development. *Journal of Hydrometeorology*, 4, 552–569.

Froidevaux, P., Schlemmer, L., Schmidli, J., Langhans, W. and Schär, C. (2014) Influence of the background wind on the local soil moisture–precipitation feedback. *Journal of the Atmospheric Sciences*, 71, 782–799. https://doi.org/10.1175/jas-d-13-0180.1.

Futyan, J.M. and Del Genio, A.D. (2007) Deep convective system evolution over Africa and the tropical Atlantic. *Journal of Climate*, 20, 5041–5060. https://doi.org/10.1175/jcli4297.1.

Gantner, L. and Kalthoff, N. (2010) Sensitivity of a modelled life cycle of a mesoscale convective system to soil conditions over West Africa. *Quarterly Journal of the Royal Meteorological Society*, 136, 471–482. https://doi.org/10.1002/qj.425.

Hohenegger, C., Brockhaus, P., Bretherton, C.S. and Schar, C. (2009) The soil moisture–precipitation feedback in simulations with explicit and parameterized convection. *Journal of Climate*, 22, 5003–5020. https://doi.org/10.1175/2009jcli2604.1.

Houze, R.A., Jr. (2004) Mesoscale convective systems. *Reviews Geophysics*, 42, RG4003. https://doi.org/10.1029/2004RG000150.

Huffman, G.J., Bolvin, D.T., Nelkin, E.J., Wolff, D.B., Adler, R.F., Gu, G., Hong, Y., Bowman, K.P. and Stocker, E.F. (2007) The TRMM multisatellite precipitation analysis (TMPA): quasi-global, multiyear, combined-sensor precipitation estimates at fine scales. *Journal of Hydrometeorology*, 8, 38–55. https://doi.org/10.1175/JHM560.1.

Joyce, R.J., Janowiak, J.E., Arkin, P.A. and Xie, P. (2004) CMORPH: a method that produces global precipitation estimates from passive microwave and infrared data at high spatial and temporal resolution. *Journal of Hydrometeorology*, 5, 487–503. https://doi.org/10.1175/1525-7541.

Lauwaet, D., van Lipzig, N.P.M., Van Weverberg, K., De Ridder, K. and Goyens, C. (2012) The precipitation response to the desiccation of Lake Chad. *Quarterly Journal of the Royal Meteorological Society*, 138, 707–719. https://doi.org/10.1002/qj.942.

Liersch, S., Cools, J., Kone, B., Koch, H., Diallo, M., Reinhardt, J., Fournet, S., Aich, V. and Hattermann, F.F. (2013) Vulnerability of rice production in the inner Niger Delta to water resources management under climate variability and change. *Environmental Science & Policy*, 34, 18–33. https://doi.org/10.1016/j.envsci.2012.10.014.

Mathon, V., Laurent, H. and Lebel, T. (2002) Mesoscale convective system rainfall in the Sahel. *Journal of Applied Meteorology*, 41, 1081–1092.

Mitsch, E.J. and Gosselink, J.G. (2015) *Wetlands*. Hoboken, NJ: Wiley.

Mohamed, Y.A., Savenije, H.H.G., Bastiaanssen, W.G.M. and van den Hurk, B. (2006) New lessons on the Sudd hydrology learned from remote sensing and climate modeling. *Hydrology and Earth System Sciences*, 10, 507–518.

Mohamed, Y.A., van den Hurk, B. J. J. M., Savenije, H.H.G. and Bastiaanssen, W.G.M. (2005) Impact of the Sudd wetland on the Nile hydroclimatology. *Water Resources Research*, 41(8), W08420. https://doi.org/10.1029/2004WR003792.

Negri, A.J., Adler, R.F., Xu, L.M. and Surratt, J. (2004) The impact of Amazonian deforestation on dry season rainfall. *Journal of Climate*, 17, 1306–1319.

Paiva, R.C.D., Buarque, D.C., Clarke, R.T., Collischonn, W. and Allasia, D.G. (2011) Reduced precipitation over large water bodies in the Brazilian Amazon shown from TRMM data. *Geophysical Research Letters*, 38, L04406. https://doi.org/10.1029/2010GL045277.

Papa, F., Prigent, C., Aires, F., Jimenez, C., Rossow, W.B. and Matthews, E. (2010) Interannual variability of surface water extent at the global scale, 1993–2004. *Journal of Geophysical Research: Atmospheres*, 115, D12111. https://doi.org/10.1029/2009JD012674.

Pedinotti, V., Boone, A., Decharme, B., Crétaux, J.F., Mognard, N., Panthou, G., Papa, F. and Tanimoun, B.A. (2012) Evaluation of the ISBA-TRIP continental hydrologic system over the Niger basin using *in situ* and satellite derived datasets. *Hydrology and Earth System Sciences*, 16, 1745–1773. https://doi.org/10.5194/hess-16-1745-2012.

Pielke, R.A., Sr. (2001) Influence of the spatial distribution of vegetation and soils on the prediction of cumulus convective rainfall. *Reviews of Geophysics*, 39, 151–177. https://doi.org/10.1029/1999RG000072.

Prigent, C., Matthews, E., Aires, F. and Rossow, W.B. (2001) Remote sensing of global wetland dynamics with multiple satellite data sets. *Geophysical Research Letters*, 28, 4631–4634. https://doi.org/10.1029/2001GL013263.

Prigent, C., Papa, F., Aires, F., Jimenez, C., Rossow, W.B. and Matthews, E. (2012) Changes in land surface water dynamics since the 1990s and relation to population pressure. *Geophysical Research Letters*, 39, L08403. https://doi.org/10.1029/2012GL051276.

Prigent, C., Papa, F., Aires, F., Rossow, W.B. and Matthews, E. (2007) Global inundation dynamics inferred from multiple satellite observations, 1993–2000. *Journal of Geophysical Research: Atmospheres*, 112, D12107. https://doi.org/10.1029/2006JD007847.

Prigent, C., Rochetin, N., Aires, F., Defer, E., Grandpeix, J.Y., Jimenez, C. and Papa, F. (2011) Impact of the inundation occurrence on the deep convection at

continental scale from satellite observations and modeling experiments. *Journal of Geophysical Research: Atmospheres*, 116, D24118. https://doi.org/10.1029/2011JD016311.

Rochetin, N., Couvreux, F. and Guichard, F. (2017) Morphology of breeze circulations induced by surface flux heterogeneities and their impact on convection initiation. *Quarterly Journal of the Royal Meteorological Society*, 143, 463–478. https://doi.org/10.1002/qj.2935.

Rowell, D.P. and Milford, J.R. (1993) On the generation of African squall lines. *Journal of Climate*, 6, 1181–1193.

Segal, M. and Arritt, R.W. (1992) Nonclassical mesoscale circulations caused by surface sensible heat-flux gradients. *Bulletin of the American Meteorological Society*, 73, 1593–1604.

Silva Dias, M.A.F., Silva Dias, P.L., Longo, M., Fitzjarrald, D.R. and Denning, A.S. (2004) River breeze circulation in eastern Amazonia: observations and modelling results. *Theoretical and Applied Climatology*, 78, 111–121. https://doi.org/10.1007/s00704-004-0047-6.

Taylor, C.M. (2010) Feedbacks on convection from an African wetland. *Geophysical Research Letters*, 37(5), L05406. https://doi.org/10.1029/2009GL041652.

Taylor, C.M. (2015) Detecting soil moisture impacts on convective initiation in Europe. *Geophysical Research Letters*, 42, 4631–4638. https://doi.org/10.1002/2015GL064030.

Taylor, C.M., Belušić, D., Guichard, F., Parker, D.J., Vischel, T., Bock, O., Harris, P.P., Janicot, S., Klein, C. and Panthou, G. (2017) Frequency of extreme Sahelian storms tripled since 1982 in satellite observations. *Nature*, 544, 475–478. https://doi.org/10.1038/nature22069.

Taylor, C.M., Birch, C.E., Parker, D.J., Dixon, N., Guichard, F., Nikulin, G. and Lister, G.M.S. (2013) Modeling soil moisture-precipitation feedback in the Sahel: importance of spatial scale versus convective parameterization. *Geophysical Research Letters*, 40(23), 6213–6218. https://doi.org/10.1002/2013GL058511.

Taylor, C.M., de Jeu, R.A.M., Guichard, F., Harris, P.P. and Dorigo, W.A. (2012) Afternoon rain more likely over drier soils. *Nature*, 489, 423–426. https://doi.org/10.1038/nature11377.

Taylor, C.M. and Ellis, R.J. (2006) Satellite detection of soil moisture impacts on convection at the mesoscale. *Geophysical Research Letters*, 33(3), L03404. https://doi.org/10.1029/2005GL025252.

Taylor, C.M., Gounou, A., Guichard, F., Harris, P.P., Ellis, R.J., Couvreux, F. and De Kauwe, M. (2011) Frequency of Sahelian storm initiation enhanced over mesoscale soil-moisture patterns. *Nature Geoscience*, 4, 430–433. https://doi.org/10.1038/ngeo1173.

Tian, Y. and Peters-Lidard, C.D. (2007) Systematic anomalies over inland water bodies in satellite-based precipitation estimates. *Geophysical Research Letters*, 34, L14403. https://doi.org/10.1029/2007GL030787.

Tuttle, S. and Salvucci, G. (2016) Empirical evidence of contrasting soil moisture–precipitation feedbacks across the United States. *Science*, 352, 825–828. https://doi.org/10.1126/science.aaa7185.

Wolski, P., Savenije, H.H.G., Murray-Hudson, M. and Gumbricht, T. (2006) Modelling of the flooding in the Okavango Delta, Botswana, using a hybrid reservoir-GIS model. *Journal of Hydrology*, 331, 58–72. https://doi.org/10.1016/j.jhydrol.2006.04.040.

Zaroug, M.A.H., Sylla, M.B., Giorgi, F., Eltahir, E.A.B. and Aggarwal, P.K. (2013) A sensitivity study on the role of the swamps of southern Sudan in the summer climate of North Africa using a regional climate model. *Theoretical and Applied Climatology*, 113, 63–81. https://doi.org/10.1007/s00704-012-0751-6.

How to cite this article: Taylor CM, Prigent C, Dadson SJ. Mesoscale rainfall patterns observed around wetlands in sub-Saharan Africa. *Q J R Meteorol Soc.* 2018;144:2118–2132. https://doi.org/10.1002/qj.3311